PHYSICAL REVIEW B VOLUME 47, NUMBER 1 1 JANUARY 1993-I

Vortex dynamics in two-dimensional underdamped, classical Josephson-junction arrays

H. S. J. van der Zant*
Department of Applied Physics, Delft University of Technology, P.O. Box 5046, 2600 GA Delft, The Netherlands and Department of Electrical Engineering and Computer Science, Massachusetts Institute of Technology, Cambridge, Massachusetts 02139

F. C. Fritschy
Department of Applied Physics, Delft University of Technology, P.O. Box 5046, 2600 GA Delft, The Netherlands

T. P. Orlando
Department of Electrical Engineering and Computer Science, Massachusetts Institute of Technology, Cambridge, Massachusetts 02139

J. E. Mooij
Department of Applied Physics, Delft University of Technology, P.O. Box 5046, 2600 GA Delft, The Netherlands
(Received 18 May 1992)

We present a systematic experimental study on vortex dynamics in two-dimensional Josephson-junction arrays built of underdamped single junctions in which charging effects can be neglected. Arrays in both square and triangular geometries are measured in small magnetic fields at low temperatures. We find that the whole picture of the spatial dynamics of vortices in two-dimensional arrays is analogous to the dynamics of the phase in a single junction. We study in detail the depinning current, the flux-flow resistance, and the maximum velocity of propagating vortices. Our data show that vortices in underdamped arrays, when driven with a current, experience more damping than can be explained by Ohmic-dissipation alone. A simple semiquantitative model, in which the energy lost to junctions in the wake of the moving vortices is taken into account, explains our data very well. The model shows that vortices will always experience damping no matter how underdamped the single junctions are.

I. INTRODUCTION

Two-dimensional (2D) arrays of superconducting islands weakly connected by Josephson junction have been studied extensively for the past ten years.[1] There are two important energy scales in Josephson-junction arrays, the Josephson coupling energy E_J and the charging energy E_C. Arrays with $E_J \gg E_C$ are classical arrays in which vortex dynamics plays a crucial role. Vortices move under the influence of a driving current and they can be detected as a voltage when passing between two voltage probes. Even in zero field, vortices may be present. The Kosterlitz-Thouless-Berezinskii (KTB) phase transition[2] separates a resistive high-temperature regime with free vortices and antivortices from a superconductive low-temperature regime where all vortices are bound in vortex-antivortex pairs. The transition takes place when $k_B T_{\mathrm{KTB}} \approx E_J$. For high driving currents below T_{KTB}, single vortices may be present due to current induced pairbreaking.

In a magnetic field at temperatures below T_{KTB} and for low currents, there are only vortices of one sign. Their number is determined by the applied magnetic field, in such a way that in a large array one vortex is present per $1/f$ cells. The frustration parameter f measures the strength of the applied field and is defined as the applied flux per cell divided by the flux quantum. At fractional values of f, the magnetically induced vortices form a lattice that is commensurate to the underlying junction network. Resistance dips can be seen at these values, as this interaction with the lattice effectively pins the vortices. At integer values of f, the behavior of junction arrays is expected to be same as for $f=0$, indicating that the resistance oscillates as a function of f with a period $f=1$. For small fields ($0<f\ll 1$) the mutual interactions between vortices and the collective interactions between the vortex lattice and the underlying lattice are small. Independent vortices experience the 2D periodic lattice potential so that vortices moving from one cell to the next have to overcome[3] a geometry dependent energy barrier U_{bar}. Below T_{KTB} vortices are mobile as long as $T > U_{\mathrm{bar}}/k_B$, and a resistance can be detected across the array. For lower temperatures, vortices are pinned in the lattice and flux flow now occurs at currents above a certain depinning current that is related to U_{bar}.

Most experiments in junction arrays have been performed in proximity-coupled arrays of superconductor–normal-metal–superconductor (SNS) junctions.[4,5] These arrays are always overdamped (the junction McCumber parameter $\beta_{c,j} \ll 1$) and vortex motion is viscous. Arrays made of superconductor-insulator-superconductor (SIS) tunnel junctions[6–8] can be made in the opposite underdamped limit ($\beta_{c,j} \gg 1$). Vortices can now be viewed as particles with a mass[9,10] and nonviscous motion of vortices should be expected.[11–13] Recent experiments[7] on arrays of underdamped SIS tun-

nel junctions have clearly shown the existence of a mass term in the equation of motion. More evidence for the existence of the vortex mass has been found in an experiment[14] with ballistic vortex propagation in a 2D array where no driving currents are applied. However, when driven with a current, experiments show that vortices experience more damping[7,8] than can be explained from Ohmic-dissipation in a Bardeen-Stephen-like flux-flow picture. To explain the experimental results, one has to assume that there is an additional damping mechanism. It has been suggested that moving vortices lose energy to the junctions in their wake and this energy oscillates at the plasma frequency.[7] Recent computer simulations by Bobbert[15] have qualitatively verified this picture.

In this paper, we present a systematic experimental study of the dynamics of vortices in square and triangular underdamped arrays in which charging effects can be neglected. The arrays are fabricated of all-aluminum high-quality Josephson tunnel junctions. We measure current-voltage characteristics at low temperatures in a small magnetic field. For low-resistance samples (100 Ω) depinning currents are in good agreement with the theoretical predictions. For high-resistance samples (1 kΩ and higher) we find that the apparent depinning current is equal to the retrapping current in a similar way as in the single junction theory. We also study the flux-flow regime for currents larger than the depinning current. We find that the dominant viscosity for $\beta_{c,j} \gg 1$ is indeed determined by the energy lost in the oscillations in the wake of the vortex. A simple semiquantitative model for the effective additional viscosity term due to these oscillations is in good agreement with our data. For even higher currents, jumps in the voltage occur, defining a maximum velocity for the propagation of single vortices.

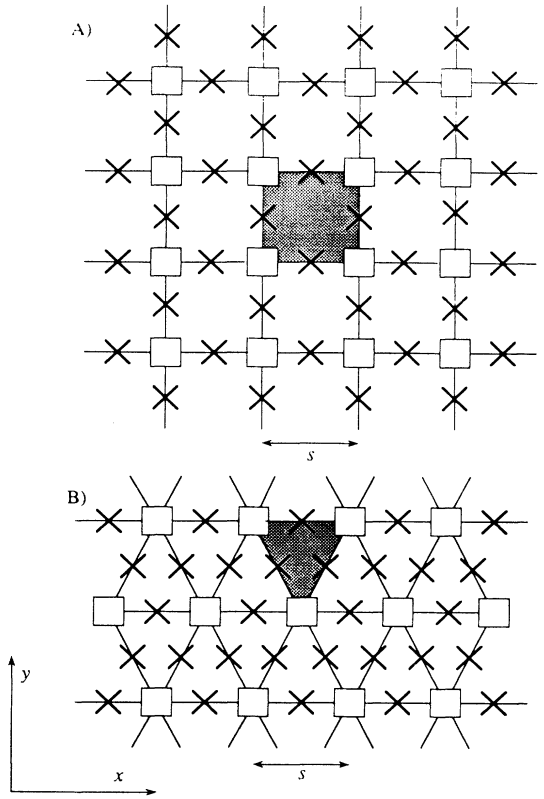

FIG. 1. A schematic drawing of a square (A) and a triangular (B) Josephson-junction array. The open squares are the superconducting islands and the crosses the Josephson junctions. The shaded areas mark cells of the arrays.

II. VORTICES IN SQUARE AND TRIANGULAR ARRAYS

Josephson-junction arrays consist of superconducting islands arranged in a regular lattice. The islands are weakly coupled to each other by Josephson junctions, as illustrated schematically in Fig. 1. In a square array, each island is connected to four neighbors; in a triangular array each island is connected to six neighbors. A cell of the array is shown in grey. In a triangular array, this is not the primitive cell, which is twice as large. The area (S) of a cell is s^2 in the square array and $\frac{1}{2}s^2$ in the triangular array, where s is the spacing between two cells in the x direction. There is an anisotropy in the triangular array. We define the average lattice constant p to be $\sqrt{S}$. For a square array $p=s$ and for a triangular array $p=s/\sqrt{(2)}$.

Below the BCS transition temperature, the islands are superconducting and the amplitude of the order parameter is constant over the whole array. Even when magnetic fields of a few flux quanta per cell are applied, the amplitude of the order parameter remains the same. Only fluctuations of its phase are relevant. In zero magnetic field the interaction energy U between two adjacent islands, $U_{mn}=E_J\cos(\phi_m-\phi_n)$. Here, ϕ_m and ϕ_n are the phases of the order parameter of islands m and n, respectively. The Josephson coupling energy E_J is proportional to the junction critical current i_c, $E_J=\Phi_0 i_c/(2\pi)$, where Φ_0 is the flux quantum, $\Phi_0=h/(2e)$. A phase difference across two adjacent nodes leads to a supercurrents through the junction connecting these two islands, which is given by $i_s=i_c\sin(\phi_m-\phi_n)$.

A perpendicular magnetic field introduces an additional phase difference A_{mn} across the junction connecting islands m and n. The quantity A_{mn} is proportional to the line integral of the vector potential $\mathbf{A}$, $A_{mn}=(2\pi/\Phi_0)\int_m^n \mathbf{A}\,dl$. In every cell of the array, summation of the A_{mn}'s must give the applied flux, i.e.,

$$\sum_{\text{cell}} A_{mn}=\frac{2\pi BS}{\Phi_0}=2\pi f\ , \tag{1}$$

where B is the magnetic field perpendicular to the plane of islands and junctions. The interaction energy and the supercurrents through the junctions are now determined by the gauge invariant phase difference $(\phi_m-\phi_n-A_{mn})$.

Vortices are special excitations in the configuration of the phases ϕ_n. The definition of a vortex (antivortex) is that following a closed contour around it, the sum of all the phase differences is 2π (-2π). In junction arrays, the 2D flux penetration depth is usually much larger than the lattice constant. The magnetic field is therefore al-

most uniform over the whole array are indicating that there is not one flux quantum in a particular cell. The defining aspect of vortices in junction arrays is therefore not the flux, but the distribution of phases. In zero field one can use the arctan analytical expression[3,5] to approximate the phase ϕ_n on island n with coordinates (x_n,y_n),

$$\phi_n=\arctan[(y_n-y_0)/(x_n-x_0)] . \quad (2)$$

In this approximation the phases point radially outward from the vortex center at (x_0,y_0). Thus, a singularity occurs in one particular cell and even within that cell the position of the vortex center can be defined with the arctan expression.

In the arctan approximation, currents around a vortex decay inversely with the distance r from its core. Vortex-vortex interactions have a long-distance character as they are proportional to $\ln(r)$. The interaction of vortices with open edges can be viewed as the attraction of a vortex with its image antivortex outside the array. In contrast, superconducting banks repel vortices, because the interaction with these edges can be viewed as the repulsion of the vortex with its image outside the array.

In underdamped arrays, one can attribute a mass to the vortices. This mass is associated with the electric energy a moving vortex generates. To calculate the mass in a quasistatic approach, equate the kinetic energy of a vortex moving with a constant terminal velocity u to the sum of the electric energy of all junctions,

$$\tfrac{1}{2}M_v u^2=\tfrac{1}{2}C\sum_{m,n}V_{mn}^2 . \quad (3)$$

Here, C is the junction capacitance. For a vortex moving from the middle of one cell to the next, the voltage across the junction connecting islands m and n, V_{mn}, can be estimated quasistatically to be

$$V_{mn}=(\Phi_0/2\pi)(u/p)(\phi_m-\phi_n) .$$

Using the arctan approximation, all the phase differences in the array can be determined numerically. In doing so for a square and triangular array, one finds the quasistatic vortex mass, M_v, to be

$$M_v=\Phi_0^2 C/2S . \quad (4)$$

This result is the same as found by others.[10] In the calculation, we have ignored the contribution proportional to the island capacitance to ground (i.e., the quasiparticle term). Recent theoretical calculations[16] indicate that in a dynamic situation the effective vortex mass can be higher by almost an order of magnitude.

Vortices in arrays move under the influence of a driving current in a direction perpendicular to the current flow. The Lorentz force associated with a driving current per junction (i_d), $F_L=\Phi_0 i_d/p$. Vortices that move from one cell to the next have to overcome an energy barrier. The height of this barrier has been determined numerically by Lobb, Abraham, and Tinkham.[3] They compared the sum of the interaction energies when the vortex is just in the middle of a cell with the one when the vortex is just in between two islands. Their quasistatic calculation gives, $U_{\rm bar}=\gamma E_J(T)$, where $\gamma=0.2$ for a large square array, and $\gamma=0.043$ for a large triangular array. For a current applied in the y direction, the potential U a vortex feels when moving in the perpendicular x direction, can well be approximated by

$$U(x)=-\tfrac{1}{2}\gamma E_J(T)\cos(2\pi x/p)-\Phi_0 i_d x/p .$$

A moving vortex also experiences a viscous drag force, $F_u=\eta u$, where η is the viscosity coefficient. In a Bardeen-Stephen-like model $\eta_{\rm BS}$ has been determined.[11] To calculate the average viscosity, one equates the energy a vortex dissipates per unit time when moving with a terminal velocity u through a viscous medium with viscosity $\eta_{\rm BS}$, to the sum of the power dissipated in each island, i.e.,

$$\eta_{\rm BS}u^2=\sum_{m,n}V_{mn}^2/r_e , \quad (5)$$

where r_e is the effective shunt resistance of each junction. With the assumption that the r_e's are the same for all junctions in the array, the summation is the same as in the calculation of the vortex mass. Hence, the result of the average Bardeen-Stephen viscosity is

$$\eta_{\rm BS}=\frac{\Phi_0^2}{2S}\frac{1}{r_e} . \quad (6)$$

In overdamped arrays, r_e is the normal-state resistance. In underdamped arrays of high-quality SIS junctions, r_e is the effective voltage-bias resistance, which is dependent on the voltage and the temperature. For low temperatures, r_e can be the subgap resistance, which is orders of magnitude higher than the normal-state resistance, indicating that vortices would then move in a medium with very little damping.

We can now combine all the previous obtained results to write down the equation of motion for a single vortex moving along a row of cells in the x direction

$$M_v\ddot{x}+\eta_{\rm BS}\dot{x}=-\frac{2\pi}{p}E_J\left[\frac{1}{2}\gamma\sin\left[\frac{2\pi x}{p}\right]-\frac{i_d}{i_c}\right] . \quad (7)$$

This equation is valid in both the square and the triangular array. By making the substitution $2\pi x/p\rightarrow\phi$, one can write Eq. (7) in the same form as the equation for the phase difference across a single junction

$$\frac{\Phi_0^2}{(2\pi)^2}\frac{C}{2}\ddot{\phi}+\frac{\Phi_0^2}{(2\pi)^2}\frac{1}{2r_e}\dot{\phi}=-\frac{1}{2}\gamma E_J\left[\sin(\phi)-\frac{i_d}{(1/2)\gamma i_c}\right] . \quad (8)$$

From this equation, one sees that the vortex dynamics in 2D arrays is equivalent to the problem of the phase difference across a single resistively and capacitively shunted junction (RCSJ) with critical current $\gamma i_c/2$, capacitance $C/2$, and shunt resistance $2r_e$. In analogy with single junctions, a McCumber parameter for vortices $\beta_{c,v}(r_e)=\gamma 2\pi i_c r_e^2 C/\Phi_0$ can be defined as well as an oscillation frequency $\omega_{p,v}=\sqrt{\gamma 2\pi i_c/\Phi_0 C}$. In square arrays

$\beta_{c,v}=0.2\beta_{c,j}$ and $\omega_{p,v}=0.44\omega_{p,j}$, where $\beta_{c,j}$ is the junction McCumber parameter, $\beta_{c,j}(r_e)=2\pi i_c r_e^2 C/\Phi_0$, and $\omega_{p,j}$ is the single junction plasma frequency, $\omega_{p,j}=\sqrt{2\pi i_c/\Phi_0 C}$. In a triangular array, $\beta_{c,v}=0.043\beta_{c,j}$ and $\omega_{p,v}=0.21\omega_{p,j}$.

The analogy between vortex dynamics and phase dynamics shows that at low temperatures the depinning current for vortices is equal to $\gamma i_c/2$. (As expected, the same answer is found by equating the Lorentz force to the maximum restoring force of the periodic lattice potential). Above the depinning current, vortex motion is expected to occur and the current-voltage characteristic to have a similar shape as the one of a single RCSJ. For underdamped vortex motion ($\beta_{c,v}>1$), the mass term in the equation of motion will lead to hysteretic vortex motion.

To calculate the flux-flow resistance, we consider a junction array of M cells long and N cells wide. The voltage due to K-independent (small fields) vortices crossing the array with a terminal velocity u is given by

$$V=\frac{\Phi_0}{2\pi}\frac{2\pi uK}{Np} . \tag{9}$$

With a 2D vortex density $n_f=K/(MNS)=f/S$, the voltage can be written as

$$V=\Phi_0 Mpun_f=\frac{\Phi_0 Muf}{p} . \tag{10}$$

For high currents, where the influence of the periodic potential is small, the equation of motion reduces to $F_L=F_u$, giving $(u/i_d)=\Phi_0/(\eta_{BS}p)$. With Eq. (6), one finds the flux-flow resistance due to a driving current through the array $I_d=(N+1)i_d$ to be

$$R_{ff}=\frac{V}{I_d}=2f\frac{M}{N+1}r_e . \tag{11}$$

III. ARRAY FABRICATION

Our all-aluminum junction arrays are made with a shadow evaporation technique. The key point of this technique is to make a mask with free hanging submicron bridges, under which Josephson tunnel junctions are formed by evaporation of superconducting material from two opposite angles. Our masks are made in a trilayer-resist system consisting of a bottom layer of 500 nm soft-baked (120 °C) AZ-1470J photoresist, and a top layer of 200 nm polymethyl methacrylate (PMMA)-10 resist baked at 105 °C. The two resist layers are separated by a 50–80 nm thick germanium layer, evaporated on a heated substrate of 100 °C. Patterns are made by direct writing in the PMMA resist with an electron-beam pattern generator. After developing, the pattern is transferred into the germanium layer by anisotropic reactive-ion etching in a SF_6 plasma. The soft-baked AZ resist is isotropically reactive-ion etched during 12 min in oxygen of 200 mbar. Under the small details of the germanium mask all the AZ resist is removed (isotropic etching) and free hanging bridges are formed. Before evaporation, the samples are wet etched in μ posit AZ developer during 10 sec, in order to remove small pieces of resist on the substrate.

Aluminum is evaporated in a conventional, diffusion pumped vacuum system with a loadlock at a rate of 0.3–0.4 nm/sec. The pressure before evaporation is typically 2×10^{-7} Torr and 5 to 10×10^{-7} Torr during evaporation. The first layer, evaporated at an angle of 45° with the substrate normal, is 28.3 nm thick, and the second layer, evaporated at an angle of −45°, is 56.6 nm. The BCS transition temperatures of these aluminum layers lie between 1.25 and 1.28 K, indicating that the aluminum is of good quality. In between the two evaporation steps, the first aluminum layer is *in situ* thermally oxidized in the load lock during 5 min. During the oxidization, the substrate holder is cooled with water of a temperature of 9–12 °C. For our evaporation system and these temperatures, we find that the normal-state junction resistivity (ρ) depends on the oxidation pressure (P_{ox}) roughly as $\rho=3.8\times10^{14}P_{ox}^{0.64}$, where ρ is expressed in Ωm^{-2} and P_{ox} in Torr. After the samples are removed out of the vacuum chamber, they are cleared by liftoff in acetone.

IV. ARRAY CHARACTERISTICS

Both square and triangular arrays of different sizes have been fabricated. Square arrays are 300 cells long ($M=300$) and 100 cells wide ($N=100$) or have $M=200$ and $N=40$. One cell in the square array has an area (S) of 50 μm^2. The triangular arrays have $L=100$ and $W=40$, and a cell area of 25 μm^2. The junctions areas (A) lie between 0.35 and 1.6 μm^2. When using the shadow evaporation technique, it is inevitable that the islands themselves are also junctions. However, the sizes of the islands are at least a factor of 15 larger than the small junctions connecting neighboring islands. The critical current of these islands junctions will be greater by the same amount, indicating that their influence will be very small.

Critical currents measured on single junctions[18] showed very good agreement with the Ambegaokar-Baratoff relation for ideal tunnel junctions,

$$i_{c,A-B}(T)r_n=[\pi\Delta(T)/2e]\tanh[\Delta(T)/(2k_BT)] .$$

The quantity $\Delta(T)$ is the temperature-dependent quasiparticle excitation gap and r_n is the normal-state junction resistance. We assume that the i_c's of the junctions in the array are given by this Ambegaokar-Baratoff relation with a BCS transition temperature T_c of 1.25 K. The array critical current I_c is defined as $I_c=(N+1)i_c$. We determine r_n from the array resistance R_n measured at 4.2 K, $r_n=R_n(N+1)/(M)$ in both the square and triangular array. For low temperatures ($T<0.5T_c$), i_c is almost temperature independent. At $T=0$, the $i_c r_n$-product is equal to 300 μV. For $T<0.5T_c$, $i_c\approx300\ \mu V/r_n$ is a useful approximation.

The junction capacitance C is estimated with the parallel plate formula, $C=\epsilon_0\epsilon_r A/t$, where ϵ_0 is the permittivity of free space, ϵ_r is the dielectric constant of the barrier, and t is the barrier thickness. For our aluminum junctions, we estimate t/ϵ_r to be 0.1 nm, leading to a

TABLE I. Sample characteristics at low temperatures for square (S) and triangular (T) arrays. M is the length of the arrays expressed in cells, r_n is the normal-state junction resistance, C is the junction capacitance, $\beta_{c,v}(r_n)$ is the vortex McCumber parameter with r_n as shunt resistance, $U_{\rm bar}$ is the vortex-energy barrier for crossing from one cell to the next, E_J/E_C is the ratio of the Josephson coupling energy to the charging energy, and λ/p is the ratio of the 2D magnetic penetration depth to the lattice constant p.

No.	Sample	M	r_n (kΩ)	C (fF)	$\beta_{c,v}(r_n)$	$U_{\rm bar}/k_B$ (K)	E_J/E_C	λ/p
S1	V2	300	0.043	160	1.3	33.1	29×10^3	5
S2	V3	300	0.08	160	2.3	18	15×10^3	10
S3	K2	100	0.08	160	2.3	18	15×10^3	10
S4	K1	100	0.011	160	3.2	13	11×10^3	14
S5	MQT2	300	3.5	35	22	0.4	76	440
S6	V6	300	3.7	80	54	0.4	166	460
S7	K4	100	14.0	160	408	0.1	88	1.8×10^3
S8	V8	300	20.6	160	600	0.07	60	2.6×10^3
S9	V8	300	48	80	700	0.03	13	5.8×10^3
T1	D5	100	0.044	65	0.11	7	11×10^3	8
T2	D4	100	0.45	65	1.1	0.7	1.1×10^3	79
T3	D8	100	0.78	65	2.0	0.4	640	137
T4	D2	100	3.08	65	7.8	0.1	162	540
T5	D7	100	3.96	65	10.1	0.08	126	690

specific junction capacitance of about 100 fF/(μm).[2] We estimate the specific island capacitance to ground to be 0.01 fF/(μm).[2] For our arrays, C is at least two orders of magnitude larger than the capacitance to ground.

The dissipation in the junction is characterized by the shunt resistance r_e, which is in general a function of temperature and voltage. In an ideal junction, dissipation is determined by tunneling of quasiparticles. For voltages larger than $2\Delta(T)/e$, there is enough energy to create quasiparticles by pairbreaking and therefore $r_e=r_n$. For voltages smaller than $2\Delta(T)/e$, the number of quasiparticles is determined by thermal activation, $r_e \propto r_n \exp(\Delta(T)/k_BT)$. At $T=T_c$, $r_e=r_n$, but for $T \ll T_c$, r_e of our aluminum junctions is orders of magnitude larger than r_n.

We estimate the geometrical inductance L_g of our cells to be about 4 pH. The junction inductance L_J is inversely proportional to the junction critical current, $L_J(T)=\Phi_0/[2\pi i_c(T)]$. At low temperatures ($T<0.5T_c$), we can write $L_J=r_n$ (in Ohms) $\times 1.1$ pH. For our arrays with $r_n>40$ Ω, $L_g i_c/\Phi_0=(L_g/2\pi L_J)<0.02$, indicating that self-field effects do not play an important role in our arrays. A similar conclusion can be drawn by looking at the 2D magnetic penetration depth $\lambda(T)=\Phi_0/[2\pi\mu_0 i_c(T)]$. Our arrays have $\lambda>5p$ even at the lowest temperatures.

In Table I, we summarize the characteristics of the arrays that have been measured. All arrays have $\beta_{c,j}(r_n)>1$ and $E_J \gg E_C$.

V. EXPERIMENTAL RESULTS

Arrays are measured in a dilution refrigerator down to 5 mK and are placed inside μ metal and leads shields. Small perpendicular fields can be applied by two coils of superconducting wire placed in a Helmholtz configuration. Electrical leads are filtered with rfi feedthrough filters at the entrance of the cryostat. For samples with a resistance higher than 200 Ω, additional filtering is applied in the mixing chamber at the low-temperature environment by means of RC and microwave filters.

Before discussing the current-voltage characteristics, we show the resistance of a square and triangular array measured as a function of applied field. These plots give an impression of the quality of the arrays. The result for a normalized temperature of $\tau=k_BT/E_J(T)=0.2$ is shown in Fig. 2. Very pronounced minima can be found for fractional values of f. For the square array, the most pronounced dip occurs at $f=\frac{1}{2}$, followed by dips at $f=\pm\frac{1}{3},\pm\frac{2}{3}$, at $f=\pm\frac{2}{5},\pm\frac{4}{5}$, and at $f=\pm\frac{1}{4},\pm\frac{3}{4}$. For the triangular array, the most pronounced dip occurs again at $f=\pm\frac{1}{2}$, but the dips at $f=\pm\frac{1}{4},\pm\frac{3}{4}$ are now deeper than the ones at $f=\pm\frac{1}{3},\pm\frac{2}{3}$. The places where the dips occur and their relative strength as measured by the depth of the dips, are in very good agreement with ground-state energy calculations of square[19] and triangular[20] arrays.

In Fig. 3, we give typical examples of low-temperature current-voltage characteristics measured at small fields. The curve in Fig. 3(a) is taken from sample T1, in which $\beta_{c,v}(r_n)<1$. The curve clearly shows the curvature characteristic for a resistively shunted junction (RSJ). In Fig. 3(b) when $\beta_{c,v}(r_n)>1$, we see hysteresis for small voltages due to the inertial mass of vortices. Once accelerated, vortices with a mass keep on moving for lower bias currents. This kind of hysteresis is found for temperatures $T<0.5$ K. (Triangular arrays with $\beta_{c,v}(r_n)>1$ show the same kind of hysteresis.) Surprisingly, we do not see the RSJ-like curvature anymore, and the flux-flow region in the I-V characteristic is almost linear with an offset of the asymptote in the positive current direction.

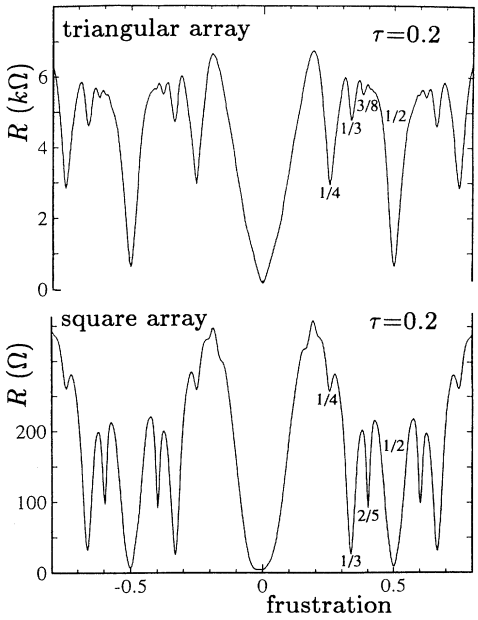

FIG. 2. The resistance of a triangular (upper curve, sample T4) and a square (lower curve, S5) Josephson-junction array measured as a function of magnetic field at a normalized temperature of 0.2. The figure shows the commensurate vortex lattices at fractional values of f as dips in the resistance.

In Fig. 3(c) the I-V characteristic of a high-Ohmic array is shown. The flux-flow region is again almost linear, but no hysteresis is observed. The low-current linear resistance in Fig. 3(c) does not vanish at $T=10$ mK. This might be due to quantum tunneling of vortices as discussed elsewhere.[7] We will not consider this low-current resistanc in this paper.

At higher currents and voltages for all samples in Fig. 3, the voltage jumps in steps to the number of rows times the gap voltage. The first jump starts at the solid circles in Fig. 3. Each step is associated with the switching of a row across the width of the array to the voltage carrying state.[21] The steps occur in a very narrow current region of at most a few percent of the maximum current, indicating that the variation in the critical current of cross rows of $(N+1)$ junctions is small. In discussing our results in more detail, we divide the remainder of this section in three parts. The first part gives the results on the depinning currents of square and triangular arrays. The second part deals with the flux-flow data from which we will determine the viscosity coefficient that vortices experience in underdamped arrays. In the last section, we show that by evaluating the voltage where the jumps start to occur, the row switching is initiated by vortices that move at a characteristic maximum velocity.

A. Depinning Currents

We define the depinning current from I-V curves as the current where the voltage across the array is equal to 2 μV. I-V characteristics are measured for different values of the temperature and the magnetic field. In Fig. 4 for sample S2, we plot the depinning currents as a function of temperature for $f=0.1$ (squares) and as a function of field for $T=10$ mK (circles). The critical currents in this figure are normalized to the temperature-dependent array critical current. For a square array the depinning current is expected to be $0.1I_c$. From the figure, one sees that the depinning current when normalized to the array critical current is almost temperature independent up to 1 K. There is a slight decrease of the depinning current below 0.5 K, which could be due to the formation of discrete energy levels in the periodic potential. These energy levels effectively lower the energy barriers and therefore the depinning currents. The energy levels are only formed at low temperatures, when all quasiparticles are frozen out. The circles, representing the depinning currents measured as a function of frustration, show that for low f the depinning currents are higher than expected. We attribute this to edge effects.[17] In our finite arrays, there exists an edge barrier for vortex entrance that vanishes for high values of f. Between $f=0.1$ and $f=0.2$, the depin-

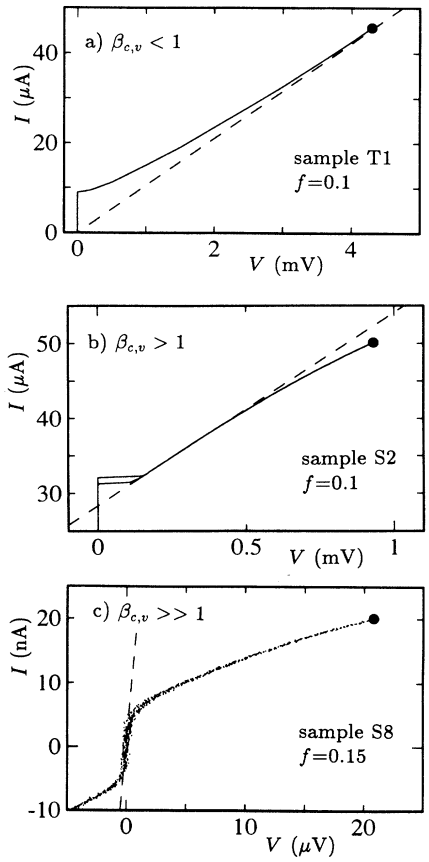

FIG. 3. Typical current-voltage characteristics of 2D Josephson-junction arrays, measured in a small magnetic field at $T=10$ mK. (a) shows the I-V characteristic for overdamped vortex motion, (b) for underdamped vortex motion, and (c) is the I-V for highly underdamped vortex motion in an array with a high normal-state resistance. At the solid circles, the voltage starts to jump (row-switching).

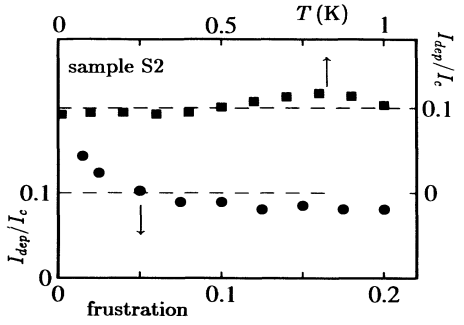

FIG. 4. The depinning current normalized to the temperature-dependent critical current as a function of temperature for $f=0.1$ (squares) and as a function of frustration for $T=10$ mK (circles). Dashed lines give the expected depinning current of $0.1I_c$.

ning current is almost constant.

On all our square and triangular arrays we have determined the depinning currents at $T=10$ mK and at $f=0.15$. The result is shown in Fig. 5, where the normalized depinning currents are plotted as a function of the vortex McCumber parameter calculated with r_n as shunt resistance. For $\beta_{c,v}<5$, we find depinning currents that are very close to the intrinsic depinning currents predicted in Sec. II (solid lines). For higher $\beta_{c,v}$ values, the depinning currents are systematically lower. This has also been seen in single junctions with high normal-state resistances.[22] and it has been shown that the retrapping current plays the role of the apparent critical current. For high-Ohmic samples, thermal fluctuations start to play an important role, even at the lowest temperatures. The fluctuations lower the critical current, but increase the retrapping current. At some point, the critical current and the retrapping current become the same, so that there is no hysteresis [Fig. 3(c)].

For a single junction, the retrapping current i_r in the absence of thermal fluctuations and for high $\beta_{c,j}$ values is given by $i_r/i_c=4/(\pi\sqrt{\beta_{c,j}})$. For vortices in 2D arrays, we can calculate $I_{\rm dep}$ as the retrapping current in a similar way as done in the single junction McCumber theory. Dashed lines in Fig. 5 give the results. We find

$$\frac{I_{\rm dep}}{\gamma I_c/2}=\frac{4}{\pi}\frac{c_1}{\sqrt{\beta_{c,v}(r_n)}}\ , \tag{12}$$

where c_1 is 2 for the square arrays and 0.4 for the triangular arrays. To compare these values of c_1 with theoretical predictions, one has to take into account thermal fluctuations and to know accurately the value of the damping resistance. However, the damping resistance in SIS arrays, which are not externally shunted, is unknown. For the high $\beta_{c,v}$ points, it cannot be excluded that depinning is caused by quantum tunneling of vortices (see discussion elsewhere[7]).

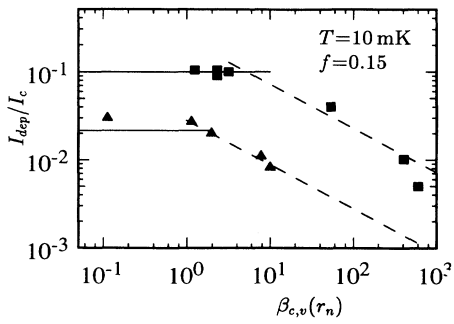

FIG. 5. The depinning currents normalized to the critical current of different square (solid squares) and triangular (solid triangles) arrays as a function of the vortex McCumber parameter calculated with r_n as shunt resistance. The depinning currents are obtained from I-V characteristics measured at $T=10$ mK and $f=0.15$. Depinning currents are defined as the current where the voltage across the array is equal to 2 μV. Solid lines give the expected depinning currents, and dashed lines the retrapping currents as obtained from the analogy with the single junction McCumber theory.

B. Flux-flow resistance

With a lock-in technique, we measure the dynamic resistance (dV/dI) as a function of frustration. For sample S2 the result at $T=10$ mK is given in Fig. 6. The flux-flow resistance is proportional to the applied field in the range $0.02<f<0.2$, but the straight line does not go through the origin as expected from ideal flux-flow theory. For $f<0.02$, we do not observe flux flow in the I-V characteristics. Again, we attribute this to edge effects.[17] (For frustrations of the order of $1/N$ and smaller there is still an entry barrier for vortices.) For $f>0.2$, the commensurate vortex lattices become visible as dips in the resistance. We have taken the straight line in Fig. 6 to obtain the effective array shunt resistance, $R_e=Mr_e/(N+1)$ [Eq. (11)]. For sample S2, we find that R_e is $1.2R_n$. This value is almost temperature independent for $T<0.6$ K. The observation that the effective damping resistance in this sample is the normal-state resistance might be due to the fact that the plasma frequency of the single junctions is of the same order as the gap frequency. For samples with a higher resistance, the plasma frequency becomes smaller and one should expect

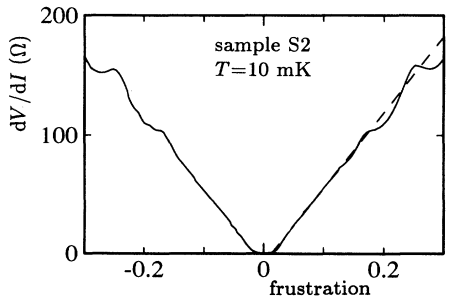

FIG. 6. The dynamic resistance of sample S2 measured as a function of frustration at $T=10$ mK. The dashed line defines an effective damping resistance of the array.

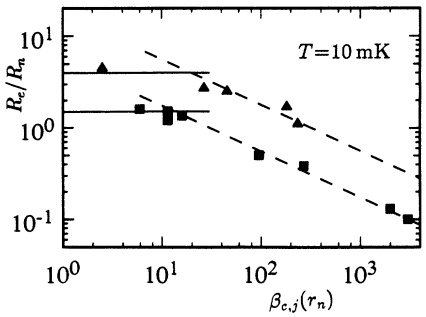

FIG. 7. The effective damping resistance measured for different samples plotted vs the junction McCumber parameter calculated with r_n as shunt resistance. The dashed lines define effective viscosities for underdamped square and triangular arrays [Eq. (13)].

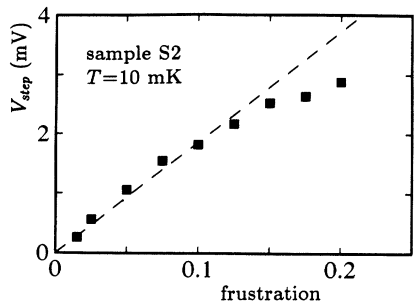

FIG. 8. The voltage where the jump to the gap voltage starts to occur as a function of frustration. The dashed line defines a maximum velocity of propagating vortices.

a higher value of the ratio R_e/R_n.

In a similar way as described above we have measured the dynamic resistance at low temperatures for the other arrays. Again we find straight lines for f in the range $0.02-0.04<f<0.2$, where the lower value depends on the array sizes. The value of 0.04 is found for our smallest arrays. In Fig. 7, we plot R_e/R_n as a function of the junction McCumber parameter. For low $\beta_{c,j}$ values, drawn lines give the predictions from the Bardeen-Stephen flux-flow model [Eq. (11)] with an effective resistance of $1.6R_n$ for the square arrays and $4R_n$ for the triangular arrays. Vortices in triangular arrays are driven with a relatively smaller current (because the depinning current is a factor 5 smaller) in which case the voltage-biased resistance can be higher. However, the most surprising result of Fig. 7 is that as $\beta_{c,j}$ increases, the ratio of the effective resistance to R_n systematically decreases. For the square arrays, we find that the effective resistance becomes even smaller than the normal-state resistance. This cannot be explained by the Bardeen-Stephen model for flux flow. In that model, the main dissipation takes place in the junction that the vortex crosses. The resistance of that junction cannot be lower than r_n. This indicates that there is an additional damping mechanism other than Ohmic-dissipation. From the dashed lines in Fig. 7, one can obtain the effective viscosity coefficient of this mechanism. We find

$$\eta=\frac{1}{c_2}\frac{\Phi_0^2}{2S}\frac{1}{\sqrt{L_J/C}}\ , \tag{13}$$

where $c_2=5.5$ for the square arrays and 9 for the triangular arrays. We will come back to this result in the next section.

C. Maximum vortex velocity

When I-V characteristics are measured for different values of f, we find that the voltage ($V_{\rm step}$) at which the first row switches depends on the magnetic field. From the I-V characteristics we have determined $V_{\rm step}$ and plotted them as a function of f. Figure 8 shows the result for sample S2. A linear dependence of $V_{\rm step}$ on f is found for small values of f (dashed line in Fig. 8). According to Eq. (10), the slope of the straight line defines a maximum vortex velocity ($u_{\rm max}$). For sample S2 we find that $u_{\rm max}=0.13p\omega_{p,j}$. In single long Josephson junctions, the vortex velocity is limited by the phase velocity of propagating electromagnetic waves.[23] Numerical simulations on 2D arrays by Nakajima and Sawada[24] also showed the existence of a maximum velocity. Their result of the maximum velocity in a square array, where self-field effects can be neglected, is $u_{\rm max}=p\omega_{p,j}/\sqrt{2}$. In numerical simulations, Bobbert[15] also found a limiting velocity for propagation of single vortices. He found that for a velocity close to $p\omega_{p,j}$, vortices and antivortices are generated in the wake of the moving vortex. The creation of vortices and antivortices triggers the switching of a row to the voltage carrying state (single-row switching).

The maximum vortex velocities normalized to $p\omega_{p,j}$ are plotted in Fig. 9 for all our arrays. The open symbols give the values of the calculations of Bobbert, and the solid symbols our experimental values. Our measured points are much lower than the ones found in the simulations and follow a different dependence on $\beta_{c,j}(r_n)$. The dashed line through the data points of the square arrays

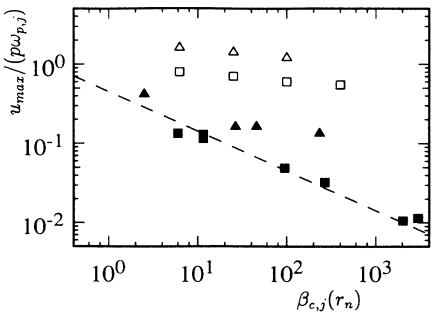

FIG. 9. Maximum vortex velocities as a function of the junction McCumber parameter calculated with r_n as shunt resistance. The solid symbols are the vortex velocities obtained from our arrays measured at $T=10$ mK and the open symbols are the vortex velocities as observed in the simulations of Bobbert (Ref. 15). The dashed line through the data points of our square arrays defines a maximum vortex velocity, $u_{\rm max}=p/(2r_nC)$.

defines a maximum velocity for our arrays, $u_{\max}/p=1/(2r_nC)$. In underdamped arrays, r_nC is the largest time constant and apparently this time scale limits the vortex velocity in highly underdamped arrays. The difference between the simulations and the experiment is probably due to the fact that in the simulations only one vortex in an array with periodic boundary conditions is studied whereas fMN vortices are present in our arrays with finite sizes.

VI. DISCUSSION AND CONCLUSION

Summarizing our experimental results, we find that the whole picture of vortex depinning and motion in 2D underdamped arrays is closely analogous to the dynamics of the phase in a single underdamped junction. Hysteresis in the current-voltage characteristics shows the importance of the inertial mass in the vortex dynamics. The most surprising result is that vortices in underdamped arrays do not move in a medium with little damping. Next to the Bardeen-Stephen viscosity term, our data show the existence of an additional viscosity term.

It has been suggested[7] that plasma oscillations in the wake of the vortex are responsible for the lost energy. Here, we present a simple model to calculate the effective viscosity due to this process. When in a square array a vortex moves from the middle of one cell to the middle of the next cell, the phase difference $\Delta\phi$ across the junction it crosses, changes by $\Delta\phi=\pi$. In a triangular array $\Delta\phi=2\pi/3$. Suppose that this is an average phase difference and that the phases of the junctions at the same time also oscillates with the plasma frequency. We can then write for the time dependent phase difference across the junction

$$\phi(t)=\phi(0)+\frac{u\Delta\phi}{p}t+D\sin(\omega_{p,j}t)\ , \tag{14}$$

where $\phi(0)=\pi/2$ in a square array, $\phi(0)=\pi/3$ in a triangular array, and where D is the amplitude of the oscillation. By demanding that $(\delta\phi/\delta t)\sim V\geq 0$ (no power extracted from the moving vortex), we find the maximum value of $D_{\max}=u\Delta\phi/(p\omega_{p,j})$. The corresponding energy of this plasma oscillation is $D_{\max}E_J$ for one cell. The number of cells that a vortex crosses per unit time is u/p, so that the total power stored in the plasma oscillations is $D_{\max}E_Ju/p$. (This power is then dissipated in the cell over a time scale, probably the r_nC time of the junction.)

Another argument for the energy stored in the oscillation is as follows. If the oscillating part of the junction is modeled by a parallel circuit of L_J and C, then a voltage, $V=(\Phi_0u\Delta\phi)/(2\pi p)$, is across this circuit for a time p/u. After this time $V=0$, so that the response to this voltage step is

$$V(t)=(\Phi_0u\Delta\phi)/(2\pi p)\cos(\omega_{p,j}t)\ .$$

This oscillating voltage produces a phase,

$$(u\Delta\phi)/(p\omega_{p,j})\sin(\omega_{p,j}t)\ ,$$

so that the total phase due to the constant and oscillating voltage is

$$\phi(t)=\phi(0)+(u\Delta\phi/p)t+(u\Delta\phi/p\omega_{p,j})\sin(\omega_{p,j}t)\ ,$$

which agrees with the $D_{\max}$ that was found.

Equating the total power of $D_{\max}E_Ju/p$ to the power (ηu^2) a vortex dissipates in a medium with effective viscosity η, one finds that the effective viscosity due to the plasma oscillations is

$$\eta_{\rm pl}=\frac{1}{c_3}\frac{\Phi_0^2}{2S}\frac{1}{\sqrt{L_J/C}}\ , \tag{15}$$

where $c_3=2\pi$ for a square array and $c_3=3\pi$ for a triangular array. These values are very close to the ones we find in our experiment (5.5 and 9, respectively).

To compare this viscosity coefficient with the Bardeen-Stephen viscosity coefficient, we calculate the ratio between them. We find

$$\eta_{\rm pl}/\eta_{\rm BS}=(1/c_3)\sqrt{\beta_{c,j}(r_n)}\ . \tag{16}$$

Thus, the more underdamped the arrays are, the more dominant the damping due to energy lost in the wake of the vortex becomes. From Eq. (15), one sees that the effective damping resistance of the second damping mechanism is $c_3\sqrt{L_J/C}$ defining an effective McCumber parameter

$$\beta_c=c_3^2\ . \tag{17}$$

This indicates that the effective McCumber parameter in square arrays cannot be higher than 40 and in triangular arrays, 89. This result, however, is obtained from the measurement on the flux-flow resistance and one should be careful with applying this result more generally. Clearly, in the measurements of the depinning currents we do not see a saturation of the effective damping.

The additional damping mechanism seems to preclude ballistic propagation of vortices in 2D underdamped arrays as observed in a recent experiment.[14] However, the experiments in this paper all deal with vortices that are driven by a transport current. The situation might be different when this transport current is absent and vortices move at low velocities. It could well be that in that case the coupling to the plasma oscillations is much weaker than when the vortices are driven with a high current. Indications for a velocity dependent damping resistance have been found in our experiments on the 2D arrays when comparing the results from the depinning current and the flux-flow resistance. The fact that the ballistic motion has been observed in triangular arrays, where the energy barriers for crossing from one cell to the next are a factor 5 smaller than in the square array, might be of importance. It could also be that the ballistic motion is due to a quantum process, i.e., that the energy transfer to the oscillations is quantized. The unit of the energy quantum is probably $\hbar\omega_{p,j}$, so that below a temperature of $\hbar\omega_{p,j}/k_B$ and for small or zero applied currents, there would be no coupling to the oscillations. Vortices would then move in an environment with very little damping. Clearly, more research on vortices in 2D arrays is needed to reveal their full dynamical behavior.

Note added in proof. Recent theoretical calculations[25,26] support our experimental data presented in this

paper. They find that vortices moving with low velocities (smaller than $0.1p\omega_j$) do not couple to the spin waves.

ACKNOWLEDGMENTS

We acknowledge valuable discussions with P. A. Bobbert, K. A. Delin, U. Eckern, W. J. Elion, R. Fazio, A. van Otterlo, and G. Schön. Samples were made at the Delft Institute of Submicron Technology (DIMES). Part of the work was supported by the Dutch Foundation for Fundamental Research on Matter (FOM) and the work at MIT was supported by NSF Grant No. DMR-9108748.

---

*Present address: Department of Electrical Engineering and Computer Science, Massachusetts Institute of Technology, Cambridge, MA 02319.

[1]For a review see Physica B **152**, 1-302 (1988).

[2]V. L. Berezinskii, Zh. Eksp. Teor. Fiz. **59**, (1970) [Sov. Phys. JETP **32**, 493 (1971)]; J. M. Kosterlitz and D. J. Thouless, J. Phys. C **6**, 1181 (1973).

[3]C. J. Lobb, D. W. Abraham, and M. Tinkham, Phys. Rev. B **27**, 150 (1983).

[4]D. J. Resnick, J. C. Garland, T. T. Boyd, S. Shoemaker, and R. S. Newrock, Phys. Rev. Lett. **47**, 1542 (1981); D. W. Abraham, C. J. Lobb, M. Tinkham, and T. M. Klapwijk, Phys. Rev. B **26**, 5268 (1982); D. Kimhi, F. Leyvraz, and D. Ariosa, *ibid.* **29**, 1487 (1984); R. K. Brown and J. C. Garland, *ibid.* **33**, 7827 (1986); C. Leeman, P. Lerch, G. A. Racine, and P. Martinoli, Phys. Rev. Lett. **56**, 1291 (1986); J. P. Carini, Phys. Rev. B **38**, 63 (1988).

[5]M. S. Rzchowski, S. P. Benz, M. Tinkham, and C. J. Lobb, Phys. Rev. B **42**, 2041 (1990).

[6]R. A. Webb, R. F. Voss, G. Grinstein, and P. M. Horn, Phys. Rev. Lett. **51**, 690 (1983).

[7]H. S. J. van der Zant, F. C. Fritschy, T. P. Orlando, and J. E. Mooij, Phys. Rev. Lett. **66**, 2531 (1991).

[8]T. Tighe, A. T. Johnson, and M. Tinkham, Phys. Rev. B **44**, 10286 (1991).

[9]E. Simanek, Solid State Commun. **48**, 1023 (1983); S. E. Korshunov, Physica B **152**, 261 (1988); A. I. Larkin, Yu. N. Ovchinikov, and A. Schmid, *ibid.* **266**, (1988).

[10]U. Eckern and A. Schmid, Phys. Rev. B **39**, 6441 (1989).

[11]T. P. Orlando, J. E. Mooij, and H. S. J. van der Zant, Phys. Rev. B **43**, 10218 (1991).

[12]B. J. van Wees, Phys. Rev. Lett. **65**, 255 (1990).

[13]T. P. Orlando and K. A. Delin, Phys. Rev. B **43**, 8717 (1991).

[14]H. S. J. van der Zant, F. C. Fritschy, T. P. Orlando, and J. E. Mooij, Europhys. Lett. **18**, 343 (1992).

[15]P. A. Bobbert, Phys. Rev. B **45**, 7540 (1992).

[16]R. Fazio, U. Geigenmüller, and G. Schön, in *Quantum Fluctuations in Mesoscopic and Macroscopic Systems,* edited by H. A. Cerdeira *et al.* (World Scientific, Singapore, 1991), p. 214.

[17]H. S. J. van der Zant, H. A. Rijken, and J. E. Mooij, J. Low Temp. Phys. **82**, 67 (1991).

[18]L. J. Geerligs, Ph.D. thesis, Delft University, 1990 (unpublished).

[19]S. Teitel and C. Jayaprakask, Phys. Rev. Lett. **51**, 1991 (1983).

[20]W. Y. Shih and D. Stroud, Phys. Rev. B **28**, 6575 (1983); D. Stroud and W. Y. Shih, Mater. Sci. Forum **4**, 177 (1985).

[21]H. S. J. van der Zant, C. J. Muller, L. J. Geerligs, C. J. P. M. Harmans, and J. E. Mooij, Phys. Rev. B **38**, 5154 (1988).

[22]M. Iansiti, A. T. Johnson, W. F. Smith, H. Rogalla, C. J. Lobb, and M. Tinkham, Phys. Rev. Lett. **59**, 489 (1987).

[23]K. K. Likharev, *Dynamics of Josephson Junctions and Circuits* (Gordon and Breach, New York, 1986).

[24]K. Nakajima and Y. Sawada, J. Appl. Phys. **52**, 5732 (1981).

[25]U. Geigenmüller, C. J. Lobb, and C. B. Whan, this issue, Phys. Rev. B **47**, 348 (1993).

[26]U. Eckern and E. B. Sonin, this issue, Phys. Rev. B **47**, 505 (1993).